Original scientific paper

ANALYTIC APPROXIMATE SOLUTION FOR NONLINEAR DYNAMICMODELING OF THE ROTATING ELASTIC 2D BEAM WITH A SINGLE CRACK

Arash Tavakoli Maleki[1], Milad Azimi[2], Samad Moradi[3]

[1]K.N. Toosi University of Technology, Tehran, Iran
[2]Aerospace Research Institute (Ministry of Science, Research, and Technology), Tehran, Iran
[3]Islamic Azad University, North Tehran Branch, Tehran, Iran

Abstract. *In this paper, the 2D lateral vibration analysis of a rotating cracked beam as a rotary structure is investigated through the Homotopy perturbation analysis and compared with the numerical Newmark-beta (Nβ) algorithm. The structure and crack are modeled as the Euler-Bernoulli (EB) theory and simple torsional spring, respectively. The nonlinear equations of motion are derived using Galerkin and the Assumed Mode Method (AMM). The system's stability is analyzed through phase plane and time response for different angular velocities of the base, initial values, external disturbances, crack stiffness, and locations. A comparative study presents simulation results for free (first nonlinear frequency) and forced vibration. It is shown that the proposed semi-analytical approach is beneficial as it provides a benchmark for a more precise analysis and further investigation of cracked rotary structures.*

Key Words: *Assumed Mode, Crack, Homotopy Perturbation, Newmark-beta, Nonlinear Vibration, Rotating Beam*

1. INTRODUCTION

   Dynamic modeling and vibration analysis of rotating structures, including rotor blades, helicopters, flexible spacecraft, flexible link manipulators, wind turbines, etc. (for aviation, space, and power generation industries), have been extensively studied. However, they neglect some concerns or factors using approximations in the modeling procedure. Several studies have been concerned with getting simplified solutions for a free and forced vibration analysis of rotating structures [1-3]. These approaches reduce

computational actions and degrees of freedom, while the accuracy incorporates the nonlinear behavior of systems remains. One of the common structural nonlinearity sources is caused by cracks [4, 5]. The structural members, particularly rotating structures, may experience internal/external disturbances that may result in structural cracks. The stiffness of the cracked structure is reduced locally; as a result, the stability and dynamic behaviors of the system are affected by crack characteristics and location. Therefore, exact modeling of the defected structure is of great significance in predicting stability, vibration behavior, and structural health monitoring [6-8]. Numerous research studies exist on the dynamic response of structures, including cracks [9-11]. This article focuses on cracked and healthy structures with rotating bases.

The rotating EB beam with a crack at its edge considering centrifugal forces as an additional stiffness is analyzed and modeled by Yashar et al. [12]. They investigated the natural frequencies and the vibration modes along the flap and chord of the cracked rotary beam using Rayleigh-Ritz and FEM. An analytical method for the free vibration analysis of the rotating cracked Functionally Graded Materials (FGM) structure is investigated by Wei et al. [13]. The advantage of the proposed method is that the eigenvalues can be extracted with the desired number of cracks. The classical Rayleigh-Ritz method is used to investigate the effects of angular velocity, crack depth, and location, on nonlinear bending vibrations of large-amplitude rotating Timoshenko beam considering the rotational axial stiffness [14]. The crack is modeled as a torsional spring that divides the beam into two sections.

The Ritz and the differential quadrature approaches are applied to investigate the effects of crack characteristics and material properties on the linear and nonlinear frequency of the FGM based on the Timoshenko beam with different boundary conditions by Kitiporancha et al. [15]. Afshari et al. investigated the vibration modeling of the EB beam with continuous crack (not as a discontinuous torsional spring) in the presence of piezoelectric (PZT) patches. They analyzed the crack growth by applying the PZT function to the structure [16].

A quadratic B-spline FEM and Galerkin methods are used to study the free vibrations of the rotating EB beam [17]. Latalski et al. studied bending-twisting vibrations of the rotating thin-walled composite structure attached to a hub [18]. In this study, the system's partial differential equations and mathematical model are derived considering rotational inertia, material anisotropy, and transverse shear and reduced to ordinary differential equations by the Galerkin approach.

Zeng et al. analyzed axial-torsional, flap-wise-chord-wise coupled vibrations of a rotating pre-twisted beam using FEM and Hamiltonian approaches [19]. Gawryluk et al. investigated the dynamical response of a rotating composite beam with a constant velocity caused by harmonic excitation from a Macro Fiber Composite (MFC) motor by FEM [20]. In this approach, the PZT materials have been used as an additional excitation source.

Dibble et al. analyzed the aero-elastic eigenvalues of a rotating blade under a variable angular velocity and compressive loading using the boundary value problem [21]. They investigated the effect of compressive and aerodynamic loading on the reduction of the rotary blade velocity. The Rayleigh-Ritz approach is utilized to study the effects of angular velocity, hub radius, and other characteristics of a pre-twisted rotating composite blade on vibrational behavior (natural frequencies and mode shapes), considering the effects of Coriolis and centrifugal forces [22]. A dynamic analysis of rotating (EB) beam

using power series solution and numerical simulations is done considering tapering effects [23]. Different researchers also investigated the dynamic analysis of rotor blades as coupled rigid-flexible systems [24, 25].

Several analytical solutions have been presented for nonlinear vibration analysis of non-rotating structures. Using a nonlocal strain gradient theory, nonlinear vibration, bending, and buckling of functionally graded Nano beams on an elastic foundation are investigated [26]. Sedighi et al. propose a parameter expansion method (PEM) for an exact nonlinear vibration analysis of a buckled beam considering dead zone boundary conditions [27].

As can be seen from the literature, much less research on analytical approaches for vibration analysis of cracked rotating structures has been reported compared to the numerous numerical investigations of such systems. On the other hand, it is required to precisely study the effects of significant parameters on the dynamic behavior of nonlinear systems. The problem can be easily handled by driving analytical models and solving approaches, especially for complex multi-body dynamics. Therefore, new methods have been proposed to deal with nonlinear problems such as Hamiltonian [28], energy balanced [29], multiple scales [30], differential transform method [31], variation [32], and homotopy perturbation approaches [33, 34]. The Homotopy Perturbation Method (HPM) is the one that provides remarkably fast convergence with high accuracy in series solutions for highly nonlinear systems and is not restricted by the assumption of a small number that existed in conventional perturbation approaches [35-37]. Essentially, this approach is a hybrid of the traditional perturbation and homotopy approaches, which have been successfully applied to nonlinear oscillations, wave, integral, heat conduction/convection/radiation equations, dispersion equations, etc. There are several approaches with the same characteristics, such as modified HPM [38, 39], global error minimization method [40], book-keeping parameter perturbation method [41], energy balance method [42], and He's frequency formulation [43].

This study proposes a new methodology for free/forced vibration and stability analysis of a rotating cracked structure (a flexible cantilever beam attached to the rotating hub considering centrifugal stiffening effects) using a high-deformation homotopy perturbation approach (a semi-analytical method).The nonlinear partial equations of the motion of the system applying the Galerkin method lead to a nonlinear second-order ordinary differential equation (NODE). Next, a semi-analytical technique is developed to establish a more precise and reliable solution for the system's nonlinear natural frequencies and time response to study different parameter effects on the stability analysis of cracked rotating structures. The main contributions are prepared so that the 2D coupled dynamic equations of the motion of a rotating elastic cracked beam are formulated considering centrifugal stiffness while HPM (with high-order deformation configuration) with second-order approximation is constructed to solve the problem. The proposed approach serves as the foundation for generalizing and implementing the HPM for a broader class of structural dynamics problems referred to as rigid-flexible body problems.

This paper is organized as follows: The dynamic equation of the motion of the rotating cracked structure is derived in Section 2 and solved by a high-order deformation HPM in Section 3. In Section 4, numerical and analytical simulations are given and compared for verifications. Finally, in Section 5, the conclusions are drawn. The predefined styles are to be used.

2. GOVERNING EQUATIONS OF MOTION

The cracked rotating-beam configuration is shown in Fig. 1. The structural model is considered an EB isotropic and uniform cantilevered beam with density ρ, length L, cross-section area A, modulus of elasticity E, and a single-axis (about Z-direction) rotating hub with an angular velocity Ω. The crack is assumed to be perpendicular to the beam's surface and open at all times. It appears as a discontinuity that affects the structure's local stiffness, the same as a mass-less torsional spring (with stiffness k).
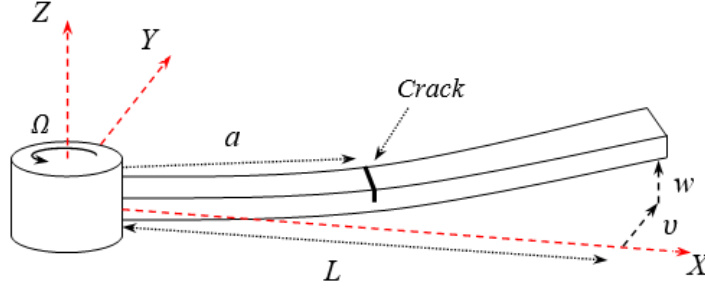

Fig. 1 Rotating cantilevered cracked structure

The three-dimensional (3D) displacement field for the EB beam is considered as:

$$u_x = u - zw' - yv' \ , \ u_y = v \ , \ u_z = w \tag{1}$$

Considering that large deformations involve nonlinear problems, the displacement strains are expressed as:

$$\varepsilon_{ij} = \frac{1}{2}\left(u_{i,j} + u_{j,i}\right) + u_{i,k}u_{j,k} \ , \ i,j,k = x,y,z \tag{2}$$

Considering $u=0$ in u_x displacement field, using the energy approach, the equations of the motion can be obtained by the Hamilton principle described by [44]:

$$\delta \int_{t_1}^{t_2} (T - U + W)dt = 0 \tag{3}$$

where T, U, and W are the kinetic, potential, and work done by the external forces, respectively, written as:

$$T = \frac{1}{2}\iiint_{\mathbb{V}} \rho |\mathbf{V}|^2 \, d\mathbb{V} = \frac{1}{2}\rho A \int_0^L \left(\dot{v}^2 + \dot{w}^2\right)dx$$

$$U = \iiint_{\mathbb{V}} \sigma_{ij}\varepsilon_{ij}\,d\mathbb{V} = \int_0^L \iint_A \sigma_{11}\left(-y\,v'' + \frac{1}{2}v''^2 - zw'' + \frac{1}{2}w''^2\right)dA\,dx$$

$$= \int_0^L -M_{zz}v'' - M_{yy}w'' + N\left\{v'^2 + w'^2\right\}dx \tag{4}$$

$$W = W_{ext} + W_R = \int_0^L \left(F_y\,\upsilon + F_z w \right) dx + \int_0^L F_R \left\{ \frac{1}{2}\upsilon'^2 + \frac{1}{2}w'^2 \right\} dx$$

$$= \int_0^L \left(F_y\,\upsilon + F_z w \right) dx - \frac{1}{2} \int_0^L \rho A \Omega^2 L^2 \left(1 - \left(\frac{x}{L} \right)^2 \right) \left\{ \upsilon'^2 + w'^2 \right\} dx$$

with:

$$M_{yy} = \iint_A \sigma_{11} z\, dA \quad,\quad M_{zz} = \iint_A \sigma_{11} y\, dA \quad,\quad N = \iint_A \sigma_{11}\, dA \tag{5}$$

where W_{ext} is the work done by external forces f_y, f_z (such as fluid or external excitation), W_R is the work done by the rotational forces (affecting the structure's stiffness). Now by proper substitution of T, U, and W into Lagrange's equation, applying the calculus of variation, the system of nonlinear differential equations of motion is obtained as:

$$\rho A \ddot{\upsilon} + EI_{zz} \upsilon'''' - \frac{AE}{2} \left[\left\{ \upsilon'^2 + w'^2 \right\} \upsilon' \right]' - \frac{1}{2} \rho A \Omega^2 L^2 \left[\left(1 - \left(\frac{x}{L} \right)^2 \right) \upsilon' \right]' = f_y(x,t)$$

$$\rho A \ddot{w} + EI_{yy} w'''' - \frac{AE}{2} \left[\left\{ \upsilon'^2 + w'^2 \right\} w' \right]' - \frac{1}{2} \rho A \Omega^2 L^2 \left[\left(1 - \left(\frac{x}{L} \right)^2 \right) w' \right]' = f_z(x,t) \tag{6}$$

Physically, a crack appears as a discontinuity in geometry and introduces considerable local flexibility. In vibration problems, the cracks can be approximated by a torsion spring [45]. Suppose that the crack only acts on the z-direction. It can divide the continuous structure into two zones. To connect these zones, considering vertical displacement, shear forces, and bending moments from equalities over both sides of the crack, we have:

$$w_1(a) = w_2(a) \ , \ w_1'''(a) = w_2'''(a) \ , \ w_2''(a) - w_1''(a) = k w_1'(a) \tag{7}$$

where k and a are the crack stiffness and location measured from the roots of the beam, respectively. It is also necessary to add four boundary conditions:

$$w_1(0) = w_1'(0) = w_1''(L) = w_1'''(L) = 0$$

$$\upsilon(0) = \upsilon_1'(0) = \upsilon_1''(L) = \upsilon_1'''(L) = 0 \tag{8}$$

with:

$$W_1(x) = A_1 \sinh(\lambda x) + B_1 \cosh(\lambda x) + C_1 \sin(\lambda x) + D_1 \sin(\lambda x)$$

$$W_2(x) = A_2 \sinh(\lambda x) + B_2 \cosh(\lambda x) + C_2 \sin(\lambda x) + D_2 \sin(\lambda x) \tag{9}$$

$$V(x) = A_3 \sinh(\lambda' x) + B_3 \cosh(\lambda' x) + C_3 \sin(\lambda' x) + D_3 \sin(\lambda' x)$$

Applying B.C for $W(x)$ and $V(x)$, determining unknown coefficients A_i and B_i in the above equation, one can remove the spatial part of the equations using the orthogonality of the linear modes. By applying the Galerkin method, the nonlinear system of PDE (NSPDE) Eq. (6) is converted to nonlinear NODE as:

$$M\ddot{T} + C\dot{T} + GT^3 + KT = F(t)$$
$$T(0) = A \ , \ \dot{T}(0) = 0$$
(10)

with:

$$M = \rho A \left\{ \int_0^L W^2(x)dx + \lambda'^4 \int_0^L V^2(x)d\varsigma \right\}$$

$$= \rho A \left\{ \left(\int_0^a W_1^2(x)dx + \int_a^L W_2^2(x)dx \right) + \lambda'^4 \int_0^L V^2(x)dx \right\}$$
(11)

$$G = \frac{AE}{2} \left\{ \int_0^L W\left((V'^2 + W'^2)W' \right)' dx + \int_0^L V\left((V'^2 + W'^2)V' \right)' dx \right\}$$

$$= \frac{AE}{2} \left\{ \int_0^a W_1\left((V'^2 + W_1'^2)W_1' \right)' dx + \int_a^L W_2\left((V'^2 + W_2'^2)W_2' \right)' dx + \int_0^L V\left((V'^2 + W'^2)V' \right)' dx \right\}$$
(12)

$$K = EI \left\{ \lambda^4 \int_0^L W^2 dx + \lambda'^4 \int_0^L V^2 dx \right\} - \frac{1}{2}\rho A\Omega^2 L^2 \left\{ \int_0^L W\left(1 - \left(\frac{x}{L}\right)^2 W' \right)' dx + \int_0^L V\left(1 - \left(\frac{x}{L}\right)^2 V \right)' dx \right\}$$

$$= EI \left\{ \lambda^4 \left(\int_0^a W_1^2 dx + \int_a^L W_2^2 dx \right) + \lambda'^4 \int_0^L V^2 dx \right\} - \frac{1}{2}\rho A\Omega^2 L^2 \left\{ \int_0^a W_1\left(1 - \left(\frac{x}{L}\right)^2 W_1' \right)' dx \right.$$
(13)

$$\left. + \int_a^L W_2\left(1 - \left(\frac{x}{L}\right)^2 W_2' \right)' dx + \int_0^L V\left(1 - \left(\frac{x}{L}\right)^2 V \right)' dx \right\}$$

$$F(t) = \int_0^L (Wf_z + Vf_y)dx = \int_0^a W_1 f_z dx + \int_a^L W_2 f_z dx + \int_0^L V f_y dx$$
(14)

and $C = \alpha M + \beta K$ as a Rayleigh damping coefficient with positive constants α and β. It is noteworthy that the integral limits defined in M, G, K, and F, as well as Eq. (7), introduce the beam as a two-part structure separated by a crack.

3. HOMOTOPY PERTURBATION SOLUTION (HIGH ORDER DEFORMATION)

In this section, we discuss the idea of HPM to solve Eq. (10). Now, let:

$$T(t) = u(\tau) \ , \ \tau = \omega t$$
(15)

Substituting Eq. (15) into the homogenous un-damped form of Eq. (10) and defining $\mathcal{K} = K/M$, $\mathcal{G} = G/M$, and $\mathcal{F} = F/M$ yields:

$$\omega^2 \ddot{u} + \mathcal{G}u^3 + \mathcal{K}u = 0$$
$$u(0) = u^* \ , \ \dot{u}(0) = 0$$
(16)

The initial solution for $u(t)$ will be:

$$u_0(t) = u^* \cos(\tau) \tag{17}$$

Constructing homotopy for Eq. (16), we have:

$$\mathbb{L}[u_m(\tau) - \mathcal{X}_m u_{m-1}(\tau)] = \hat{h}\mathcal{H}(\tau)R_m(\mathbf{u}_n) \tag{18}$$

with:

$$\mathbb{L} = \ddot{\mathcal{U}}(\tau, q) + \mathcal{U}(\tau, q) \tag{19}$$

$$R_m(\mathbf{u}_n) = \frac{\partial^{(m-1)}\mathbb{N}(\mathcal{U}(\tau, q))}{(m-1)!\partial q^{(m-1)}}\bigg|_{q=0} \tag{20}$$

$$\mathbb{N}(\mathcal{U}(\tau, q)) = \Omega^2 \ddot{\mathcal{U}} + \mathcal{G}\mathcal{U}^3 + \mathcal{K}\mathcal{U} \tag{21}$$

$$\mathcal{X}\begin{cases} 0 & m \leq 1 \\ 1 & m > 1 \end{cases} \tag{22}$$

$$\Omega = \sum_{n=0}^{\infty} \omega_n q^n \tag{23}$$

$$\mathcal{U}(\tau, q) = u_0 + \sum_{n=1}^{\infty} u_n(t)q^n = u_0 + q^1 u_1 + q^2 u_2 + \dots \tag{24}$$

where $\mathbb{N}$, $\mathbb{L}$, $\hat{h}$, q, and $\mathcal{H}(\tau)$ are nonlinear operator, linear operator, auxiliary constant, perturbation, and auxiliary parameters, respectively. For $n=1$, we have:

$$\mathbb{L}[u_1(\tau)] = \hat{h}\mathcal{H}(\tau)R_1(\mathbf{u}_n) \tag{25}$$

where:

$$R_1(\mathbf{u}_1) = \frac{\partial^0 \mathbb{N}(\mathcal{U}(\tau, q))}{\partial q^0}\bigg|_{q=0} = \omega_0^2 \ddot{u}_0 + \mathcal{G}u_0^3 + \mathcal{K}u_0 \tag{26}$$

Substituting Eq. (24) into Eq. (21) yields:

$$\ddot{u}_1 + u_1 = \omega_0^2 \ddot{u}_0 + \mathcal{G}u_0^3 + \mathcal{K}u_0 \tag{27}$$

Also, with substituting Eq. (17) into Eq. (27), we have:

$$\ddot{u}_1 + u_1 = -\omega_0^2 u^* \cos(\tau) + \mathcal{G}\left(u^* \cos(\tau)\right)^3 + \mathcal{K}u^* \cos(\tau) \tag{28}$$

with some simplification, Eq. (28) can be expressed as:

$$\ddot{u}_1 + u_1 = -\omega_0^2 u^* \cos(\tau) + \mathcal{G}u^{*3}\left(\frac{3}{4}\cos(\tau) + \frac{1}{4}\cos(3\tau)\right) + \mathcal{K}u^* \cos(\tau)$$

$$= \left(-\omega_0^2 u^* + \mathcal{K}u^* + \frac{3}{4}\mathcal{G}u^{*3}\right)\cos(\tau) + \frac{\mathcal{G}u^{*3}}{4}\cos(3\tau) \qquad (29)$$

The secular term $\cos(\tau)$ has to be eliminated for the next iterations, so its coefficient must be zero:

$$-\omega_0^2 u^* + \mathcal{K}u^* + \frac{3}{4}\mathcal{G}u^{*3} = 0 \qquad (30)$$

which results in:

$$\omega_0 = \sqrt{\mathcal{K} + \frac{3}{4}\mathcal{G}u^{*2}} \qquad (31)$$

Rewriting Eq. (29) without secular terms yields:

$$\ddot{u}_1 + u_1 = \frac{\mathcal{G}u^{*3}}{4}\cos(3\tau) \qquad (32)$$

Repeating for *n=2* and some simplification, we have:

$$\omega^2 = \left(\mathcal{K} + \frac{3}{4}\mathcal{G}u^{*2}\right)^2 + \sqrt{\mathcal{K}^2 + \frac{3}{2}\mathcal{G}\mathcal{K}u^{*2} + \frac{21}{32}\mathcal{K}^2 u^{*4}} \qquad (33)$$

$$u = u_0 + u_1 + \dots \qquad (34)$$

In order to obtain the time response analysis to external disturbance $\mathcal{F} = \mathcal{F}_0 \cos(\bar{\tau})$ of system Eq. (10), reconstructing Eq. (29) as:

$$\ddot{u}_1 + u_1 = -\omega_0^2 u^* \cos(\tau) + \mathcal{G}u^{*3}\left(\frac{3}{4}\cos(\tau) + \frac{1}{4}\cos(3\tau)\right) + \mathcal{K}u^* \cos(\tau) + \mathcal{F}_0 \cos(\bar{\tau})$$

$$= \left(-\omega_0^2 u^* + \mathcal{K}u^* + \frac{3}{4}\mathcal{G}u^{*3}\right)\cos(\tau) + \frac{\mathcal{G}u^{*3}}{4}\cos(3\tau) + \mathcal{F}_0 \cos(\bar{\tau}) \qquad (35)$$

with $\bar{\tau} = \omega_F t$, where ω_F is defined as an excitation frequency. Eliminating secular terms and rewriting Eq. (35) as:

$$\ddot{u}_1 + u_1 = \frac{\mathcal{G}u^{*3}}{4}\cos(3\tau) + \mathcal{F}_0 \cos(\bar{\tau}), \quad u_1(0) = 0, \ \dot{u}_1(0) = 0 \qquad (36)$$

The solution is given by:

$$u_1 = \left(\frac{\mathcal{G}u^{*3}}{32} + F_0\right)\cos(\tau) + \frac{\mathcal{G}u^{*3}}{32}\cos(3\tau) + F_0 \cos(\bar{\tau}) \qquad (37)$$

4. SIMULATION RESULTS

The simulation results have been investigated to study the system's performance in the main parameter variation. The effective parameters of the problem are: crack location, corresponding torsional stiffness, angular velocity, external force, and initial values. In each case, time responses and phase diagrams have been obtained. In the simulations, the physical parameters used to describe the system are considered to be: *L=12 (m)*, *E=210 (GPa)*, *ρ=7800(kg/m³)*,*A=bh=(0.6×0.04) (m²)*. The system performance in terms of fundamental nonlinear natural frequency (FNNF) is analyzed for different cases. Table 1 shows the effects of three different input base angular velocities Ω *(rad/s)* on FNNF. In this case, the equivalent torsion spring stiffness is *k=1×10⁶(N.mm/rad)*, the initial value is *u*=0.01*, and the crack location is *a=6 (m)* or *c=a/L=0.5*.

Table 1 FNNF for different angular velocities Ω

Parameter	$\Omega=0$	$\Omega=5$	$\Omega=10$
ω	0.8216	6.661	11.5759

Table 2 FNNF for different crack location *c*

Parameter	c=0.1	c=0.3	c=0.5	c=0.7	c=0.9
ω	4.294	5.433	6.661	7.373	8.169

Table 3 FNNF for different crack stiffness *k*

Parameter	$k=\infty$	$k=1e6$	$k=1e5$
ω	7.187	6.661	4.663

Moreover, the effects of crack characteristics on FNNF are shown in Tables 2 and 3, respectively. Clearly, with the increase in the angular velocity crack stiffness, the FNNF of the cracked and the uncracked beam becomes closer to each other. In addition, for cracks near the clamped boundary, the FNNF value is decreased. It can also be found that, for fixed crack properties, the FNNF increases with increasing angular velocity due to the centrifugal stiffness.

In the following, a comprehensive parameter analysis was performed to examine how the initial value, hub rotational speed, crack stiffness and crack location affect the free and force vibration responses of the system analytically and numerically. In order to demonstrate the effectiveness of the proposed approach, a comparison is carried out between HPM with high deformation and the Runge-Kutta (4th order) numerical approach. It can be seen that both methods behave similarly, with a slight deviation observed at higher deformation rates.

The system performance in the case of free vibration phase diagrams is illustrated in Figs. 2-5. In order to verify the accuracy of the HPM, the results are compared with the Nβ algorithm. As shown in Fig. 2, the system's stability is preserved for all prescribed initial values. Only the increase in amplitude can reduce the stability conditions, which means the radius of the circles (phase portraits) increases. The dimensions of circular patterns are associated with the energy equilibrium of the system. Thus, as the system's rigidity increases, each loop's size decreases.
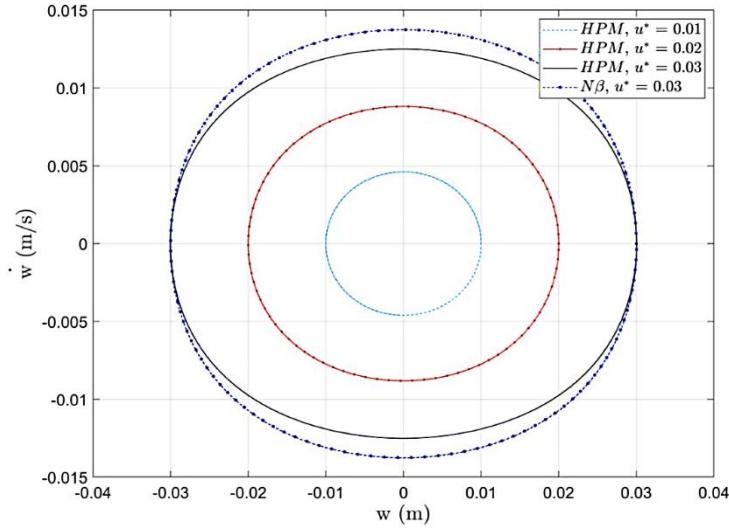
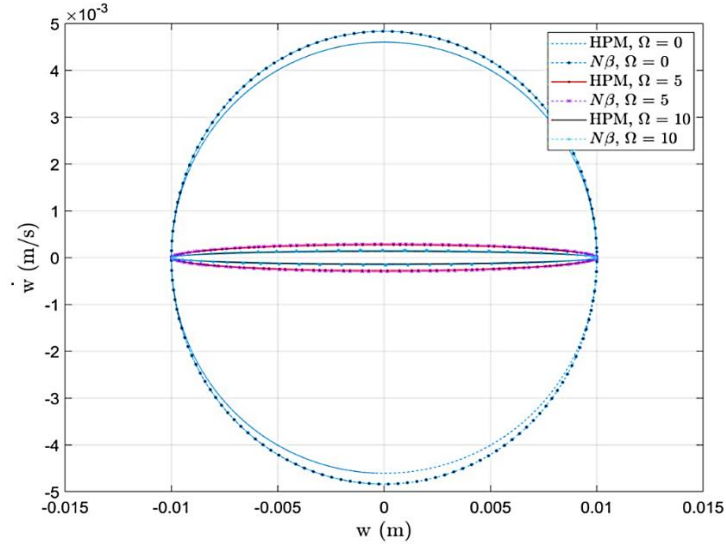**Fig. 2** Phase portrait for different u^* (free vibration)

Fig. 3 Phase portrait for different Ω (free vibration)

From Fig. 3, the circular pattern of the non-rotating structures strongly becomes elliptic by increasing the angular velocity of the base. Hence with an identical value in the vibration amplitude, the rates are sharply reduced, which indicates an increase in rotational stiffness of the system. This happens for other cases where the crack stiffness increases and the crack moves towards the structure's tip at a lower rate, as shown in Figs 4 and 5. Moreover, a relatively acceptable correspondence is observed between HPM and Nβ.
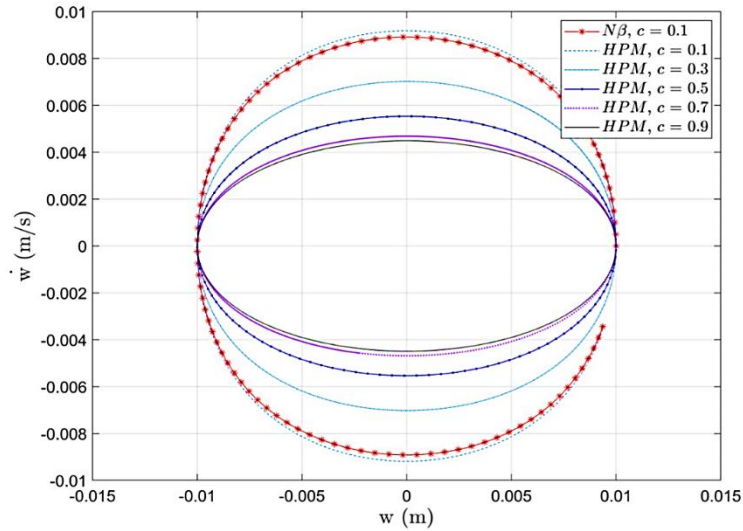
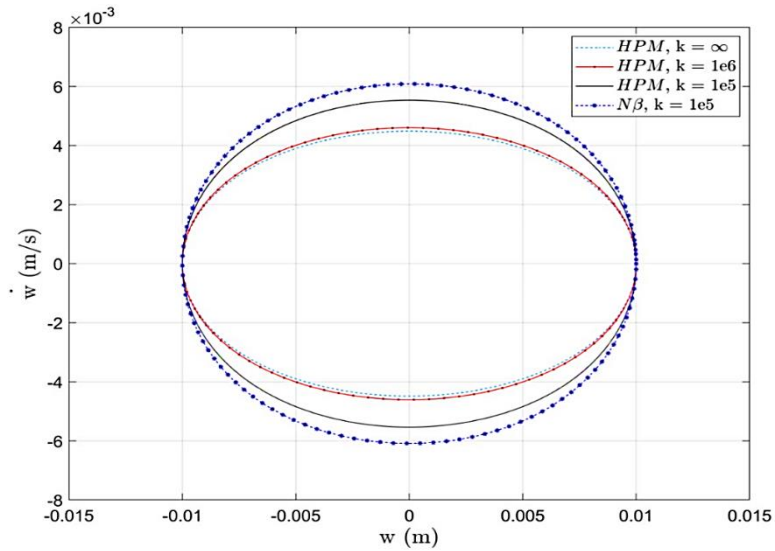**Fig. 4** Phase portrait for different c (free vibration)

Fig. 5 Phase portrait for different k (free vibration)

The simulations of forced vibration in time response (tip deflection) and phase diagrams are compared in Figs. 6-9. Similar to free vibration, the force vibration responses in phase diagrams are compared with Nβ, and again, a good agreement is observed.

It is worth noting that a general response for systems with force vibration is periodic curves with finite cycles, in which the period corresponds to the excitation type. The

effect of different parameters on the stability and performance of the system is investigated. As for the free vibration analysis, the most prominent parameter which affects the system performance in the presence of external disturbance is the angular velocity and the disturbance amplitude (Figs. 6 and 7), so that the non-rotating structure has larger tip velocities of the order of ~3.5 times compared to the rotating cases. On the other hand, by increasing the angular velocity to $\Omega=5$, we face an increase in the amplitude of the oscillations. However, there is a significant reduction in the tip amplitude and its rate as the base angular velocity reaches $\Omega=10$.
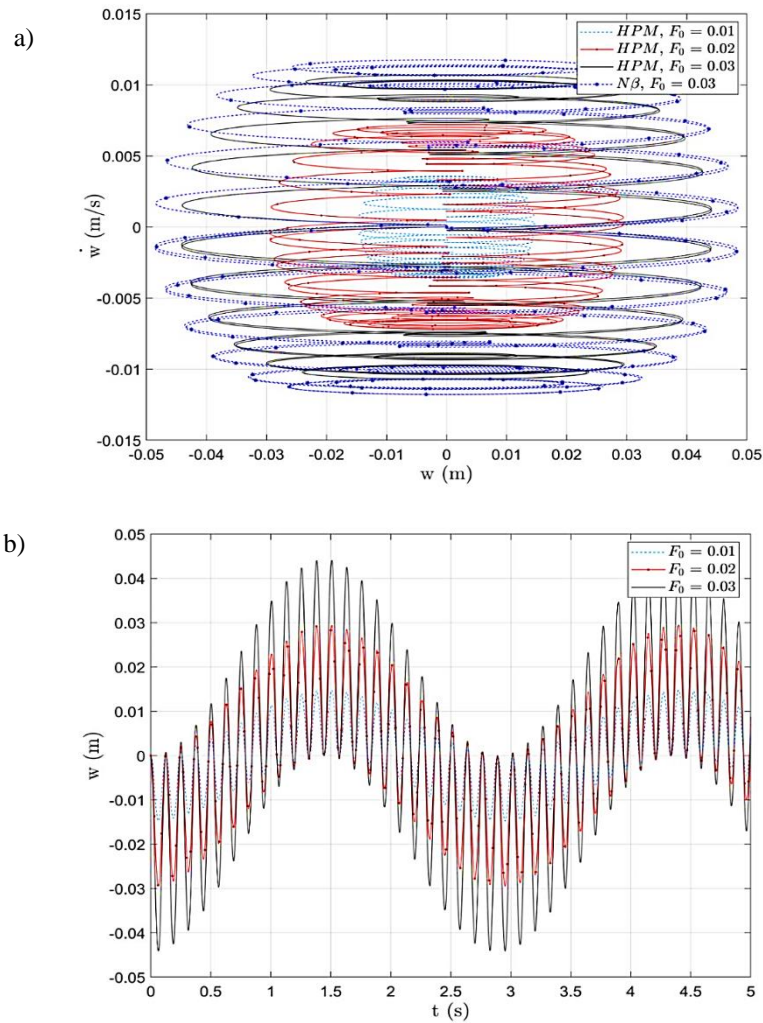

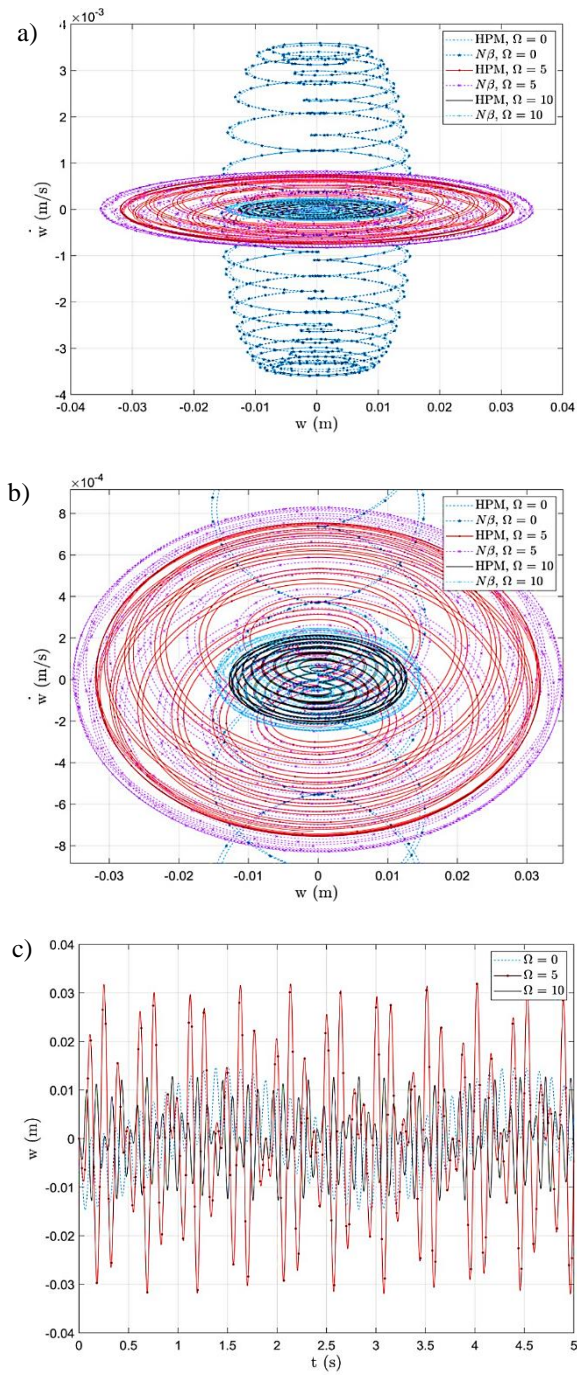**Fig. 6** Forced vibration response to F_0, a) Phase portrait b) Tip displacement

Fig. 7 Forced vibration response for different Ω, a) Phase portrait b) Phase diagram (magnified) c) Tip displacement
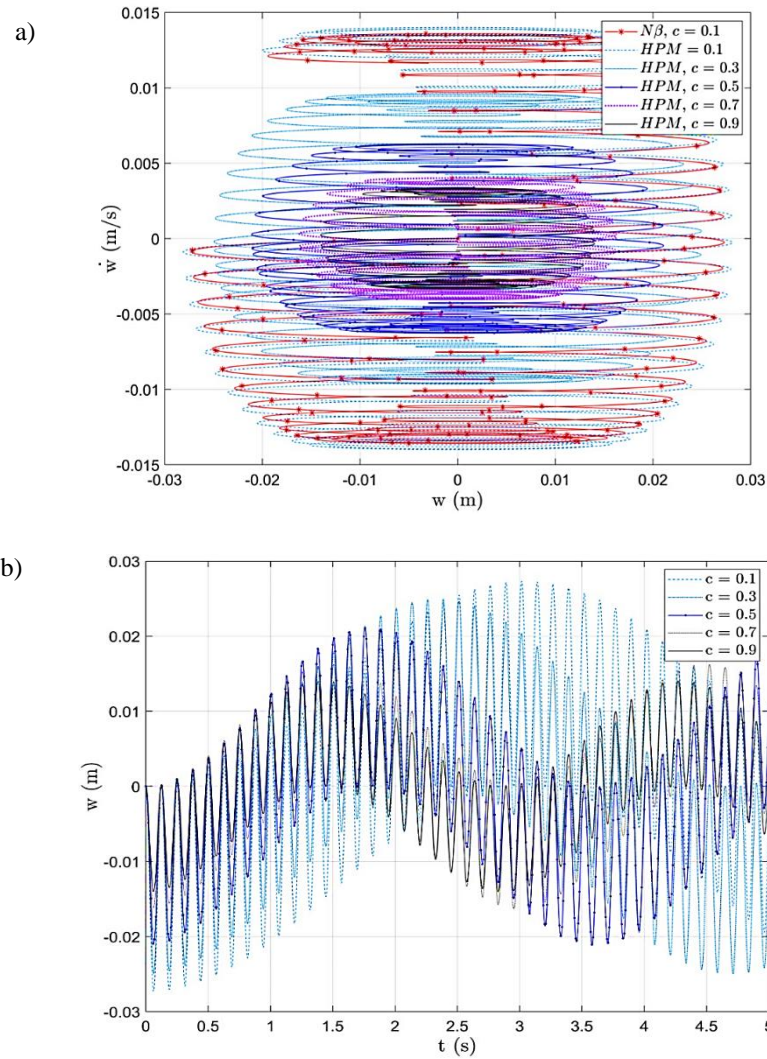
Fig. 8 Forced vibration response for different c, a) Phase portrait b) Tip displacement

It should be noted that different studies to investigate the effects of crack location and stiffness in the form of closed curves are shown in phase diagrams with a concentric but different radius. In the presence of external disturbances, as the crack gets closer to the base and as the crack stiffness increases, the radius increases, which provides that the system dynamic becomes more sensitive to parameter variations, external disturbances, and changes in the system stability criteria.

One can conclude that the phase diagram of free vibration systems shows periodic steady-state orbits whose amplitude varies with initial conditions. In contrast, for forced vibration analysis, this phase diagram represents periodic orbits characterized by a period proportional to the harmonic excitation force.
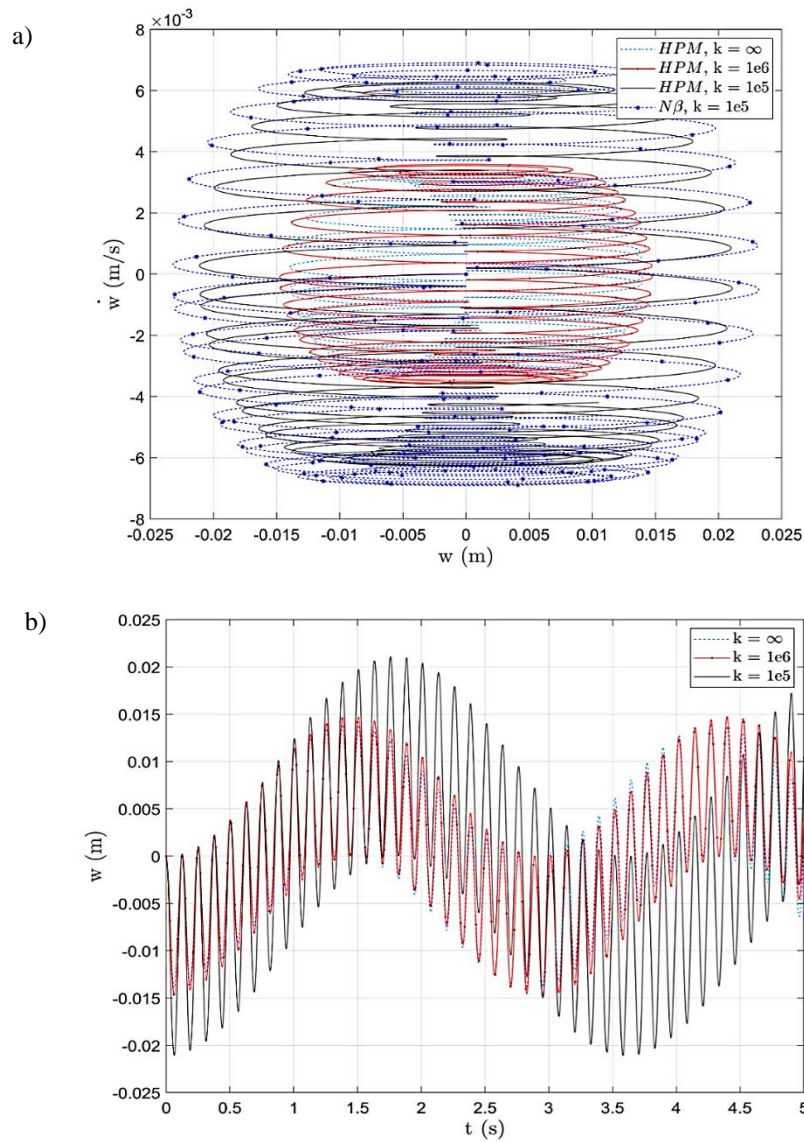
a)

b)

Fig. 9 Forced vibration response for different k, a) Phase portrait b) Tip displacement

5. CONCLUSIONS

This study analyzes the free and forced nonlinear vibration of a cracked EB beam attached to a rotating base. It is shown that the nonlinear governing ordinary differential equation can be extracted from PDE and solved using the high-order deformation form of HPM. Comprehensive investigations based on nonlinear natural frequency, time response, and the phase diagram are made to analyze the system's vibration

characteristics and stability, considering essential parameter effects such as angular velocities, external disturbances, crack characteristics and initial values. It is shown that due to the presence of axial forces (Centrifugal forces), the stability of the rotating structure is increased, so it can partly cover the crack drawbacks and can be considered a crack property-independent problem at high angular velocities. It is concluded that the HPM, even with lower-order iteration, has great potential compared to numerical approaches such as Nβ, which proposes an analytical approximation to the solutions of nonlinear structural dynamics. This research may contribute to developing, implementing, and realizing active vibration control algorithms for rotating structures in future studies. Accordingly, a rotating simulator will be considered as an experimental test bed to verify the feasibility and accuracy of the proposed approach.

REFERENCES

1. Zhou, Y., Zhang, Y., Yao, G., 2021, *Higher-order stability analysis of a rotating BDFG tapered beam with time-varying velocity,* Composite Structures, 267, 113858.
2. Saravia, C.M., Machado, S.P., Cortínez, V.H., 2011, *Free vibration and dynamic stability of rotating thin-walled composite beams,* European Journal of Mechanics-A/Solids, 30(3), pp. 432-441.
3. Bab, S., Khadem, S., Mahdiabadi, M., Shahgholi, M., 2017, *Vibration mitigation of a rotating beam under external periodic force using a nonlinear energy sink (NES),* Journal of Vibration and Control, 23(6), pp. 1001-1025.
4. Strzalka, C., Marinkovic, D., Zehn, M.W., 2021, *Stress mode superposition for a priori detection of highly stressed areas: Mode normalisation and loading influence,* Journal of Applied and Computational Mechanics, 7(3), pp. 1698-1709.
5. Gayen, D., Tiwari, R., Chakraborty, D., 2019, *Static and dynamic analyses of cracked functionally graded structural components: a review,* Composites Part B: Engineering, 173, 106982.
6. Kim, S., Kim, K., Ri, M., Paek, Y., Kim, C., 2021, *A semi-analytical method for forced vibration analysis of cracked laminated composite beam with general boundary condition,* Journal of Ocean Engineering and Science, 6(1), pp. 40-53.
7. De Rosa, M., Lippiello, M., 2021, *Closed-form solutions for vibrations analysis of cracked Timoshenko beams on elastic medium: an analytically approach,* Engineering Structures, 236, 111946.
8. Altunışık, A.C., Okur, F.Y., Karaca, S., Kahya, V., 2019, *Vibration-based damage detection in beam structures with multiple cracks: modal curvature vs. modal flexibility methods,* Nondestructive Testing and Evaluation, 34(1), pp. 33-53.
9. Yadao, A.R., Parhi, D.R., 2016, *The influence of crack in cantilever rotor system with viscous medium,* International Journal of Dynamics and Control, 4(4), pp. 363-375.
10. Batihan, A.Ç., Kadioğlu, F.S., 2016, *Vibration analysis of a cracked beam on an elastic foundation,* International Journal of Structural Stability and Dynamics, 16(05), 1550006.
11. Akbaş, Ş.D., 2017, *Free vibration of edge cracked functionally graded microscale beams based on the modified couple stress theory,* International Journal of Structural Stability and Dynamics, 17(03), 1750033.
12. Yashar, A., Ferguson, N., Ghandchi-Tehrani, M., 2018, *Simplified modelling and analysis of a rotating Euler-Bernoulli beam with a single cracked edge,* Journal of Sound and Vibration, 420, pp. 346-356.
13. Wei, D., Liu, Y., Xiang, Z., 2012, *An analytical method for free vibration analysis of functionally graded beams with edge cracks,* Journal of Sound and Vibration, 331(7), pp. 1686-1700.
14. Panigrahi, B., Pohit, G., 2018, *Effect of cracks on nonlinear flexural vibration of rotating Timoshenko functionally graded material beam having large amplitude motion,* Proceedings of the Institution of Mechanical Engineers, Part C: Journal of Mechanical Engineering Science, 232(6), pp. 930-940.
15. Kitipornchai, S., Ke, L., Yang, J., Xiang, Y., 2009, *Nonlinear vibration of edge cracked functionally graded Timoshenko beams,* Journal of sound and vibration, 324(3-5), pp. 962-982.
16. Afshari, M., Inman, D.J., 2013, *Continuous crack modeling in piezoelectrically driven vibrations of an Euler–Bernoulli beam,* Journal of Vibration and Control, 19(3), pp. 341-355.

17. Panchore, V., Ganguli, R., 2018, *Quadratic B-spline finite element method for a rotating nonuniform Euler–Bernoulli beam,* International Journal for Computational Methods in Engineering Science and Mechanics, 19(5), pp. 340-350.
18. Latalski, J., Warminski, J., Rega, G., 2017, *Bending–twisting vibrations of a rotating hub–thin-walled composite beam system,* Mathematics and Mechanics of Solids, 22(6), pp. 1303-1325.
19. Zeng, J., Ma, H., Yu, K., Xu, Z., Wen, B., 2019, *Coupled flapwise-chordwise-axial-torsional dynamic responses of rotating pre-twisted and inclined cantilever beams subject to the base excitation,* Applied Mathematics and Mechanics, 40(8), pp. 1053-1082.
20. Gawryluk, J., Mitura, A., Teter, A., 2019, *Dynamic response of a composite beam rotating at constant speed caused by harmonic excitation with MFC actuator,* Composite Structures, 210, pp. 657-662.
21. Dibble, R., Ondra, V., Woods, B.K., Titurus, B., 2019, *Aeroelastic eigenvalue analysis of a variable speed rotor blade with an applied compressive load*, in *AIAA Scitech 2019 Forum*.
22. Chen, J., Li, Q.-S., 2019, *Vibration characteristics of a rotating pre-twisted composite laminated blade,* Composite Structures, 208, pp. 78-90.
23. Adair, D., Jaeger, M., 2018, *A power series solution for rotating nonuniform Euler–Bernoulli cantilever beams,* Journal of Vibration and Control, 24(17), pp. 3855-3864.
24. Castillo-Rivera, S., Tomas-Rodriguez, M., 2018, *Helicopter modelling and study of the accelerated rotor,* Advances in Engineering Software, 115, pp. 52-65.
25. Adair, D., Jaeger, M., 2019, *Efficient Calculation of the Hingeless Rotor Blade Flap-Lag-Torsion Dynamics for Helicopters*, in *AIAA Scitech 2019 Forum*.
26. Hieu, D.V., Chan, D.Q., Sedighi, H.M., 2021, *Nonlinear bending, buckling and vibration of functionally graded nonlocal strain gradient nanobeams resting on an elastic foundation,* Journal of Mechanics of Materials and Structures, 16(3), pp. 327-346.
27. Sedighi, H.M., Shirazi, K., Noghrehabadi, A., Yildirim, A., 2012, *Asymptotic investigation of buckled beam nonlinear vibration,* Iranian Journal of Science and Technology, Transactions of Mechanical Engineering, 36(M2), pp. 107-116.
28. He, J.-H., Hou, W.-F., Qie, N., Gepreel, K.A., Shirazi, A.H., Mohammad-Sedighi, H., 2021, *Hamiltonian-based frequency-amplitude formulation for nonlinear oscillators,* Facta Universitatis. Series: Mechanical Engineering, 19(2), pp. 199-208.
29. Akbarzade, M., Farshidianfar, A., 2017, *Nonlinear transversely vibrating beams by the improved energy balance method and the global residue harmonic balance method,* Applied Mathematical Modelling, 45, pp. 393-404.
30. Ebrahimi, F., Zia, M., 2015, *Large amplitude nonlinear vibration analysis of functionally graded Timoshenko beams with porosities,* Acta Astronautica, 116, pp. 117-125.
31. Jena, S.K., Chakraverty, S., 2018, *Free vibration analysis of Euler–Bernoulli nanobeam using differential transform method,* International Journal of Computational Materials Science and Engineering, 7(03), 1850020.
32. Ansari, R., Gholami, R., Rouhi, H., 2019, *Geometrically nonlinear free vibration analysis of shear deformable magneto-electro-elastic plates considering thermal effects based on a novel variational approach,* Thin-Walled Structures, 135, pp. 12-20.
33. Sadet, J., Massa, F., Tison, T., Turpin, I., Lallemand, B., Talbi, E.-G., 2021, *Homotopy perturbation technique for improving solutions of large quadratic eigenvalue problems: Application to friction-induced vibration,* Mechanical Systems and Signal Processing, 153, 107492.
34. Huang, X., Zhang, Y., Moradi, Z., Shafiei, N., 2021, *Computer simulation via a couple of homotopy perturbation methods and the generalized differential quadrature method for nonlinear vibration of functionally graded non-uniform micro-tube,* Engineering with Computers, 38(3), pp. 2481-2498.
35. He, J.-H., El-Dib, Y.O., Mady, A.A., 2021, *Homotopy perturbation method for the fractal toda oscillator,* Fractal and Fractional, 5(3), 93.
36. He, J.H., El-Dib, Y.O., 2021, *The reducing rank method to solve third-order Duffing equation with the homotopy perturbation,* Numerical Methods for Partial Differential Equations, 37(2), pp. 1800-1808.
37. Ali, M., Anjum, N., Ain, Q.T., He, J.-H., 2021, *Homotopy perturbation method for the attachment oscillator arising in nanotechnology,* Fibers and Polymers, 22(6), pp. 1601-1606.
38. Li, X.-X., He, C.-H., 2019, *Homotopy perturbation method coupled with the enhanced perturbation method,* Journal of Low Frequency Noise, Vibration and Active Control, 38(3-4), pp. 1399-1403.
39. Anjum, N., He, J.-H., Ain, Q.T., Tian, D., 2021, *Li-He's modified homotopy perturbation method for doubly-clamped electrically actuated microbeams-based microelectromechanical system,* Facta Universitatis. Series: Mechanical Engineering, 19(4), pp. 601-612.
40. Farzaneh, Y., Tootoonchi, A.A., 2010, *Global error minimization method for solving strongly nonlinear oscillator differential equations,* Computers & Mathematics with Applications, 59(8), pp. 2887-2895.

41. He, J.-H., 2001, *Bookkeeping parameter in perturbation methods,* International Journal of Nonlinear Sciences and Numerical Simulation, 2(3), pp. 257-264.
42. Xie, K., Wang, Y., Niu, H., Chen, H., 2020, *Large-amplitude nonlinear free vibrations of functionally graded plates with porous imperfection: A novel approach based on energy balance method,* Composite Structures, 246, 112367.
43. He, J.-H., 2019, *The simplest approach to nonlinear oscillators,* Results in Physics, 15(2019), 102546.
44. Rao, S.S., 2019, *Vibration of continuous systems*. John Wiley & Sons.
45. Gounaris, G., Dimarogonas, A., 1988, *A finite element of a cracked prismatic beam for structural analysis,* Computers & Structures, 28(3), pp. 309-313.